DOI 10.2478/ama-2025-0080

ANALYSIS OF PORTEVIN-LE CHÂTELIER EFFECT DATA USING DIFFFERENT SAMPLE ENTROPY MEASURES

Marzena MUCHA*

*Chair for Computational Engineering, Faculty of Civil Engineering,
Cracow University of Technology, Warszawska 24, 31-155 Kraków

marzena.mucha@pk.edu.pl

received 11 February 2025, revised 12 November 2025, accepted 30 November 2025

Abstract: This work is focused on calculating entropy measures for signals in order to identify Portevin-Le Châtelier (PLC) effect types. The PLC effect is a phenomenon occurring in metals, in particular steel and aluminum alloys, within a certain range of strain rates and temperatures. It is characterized by serrations (repetitive changes from hardening to softening) visible in a load-displacement diagram and associated strain rate bands moving through a sample. Three main PLC types are distinguished: A, B and C. Type A occurs in low temperature and for high strain rate, strain rate bands then propagate continuously. Type B occurs for medium temperature and strain rate, the bands then have a hopping character. Type C occurs in high temperature and for low strain rate, the bands then nucleate in a random manner. The entropy analysis is used as a way to distinguish the types. The so-called Sample Entropy, Sample Entropy 2d and Multiscale Sample Entropy are measures utilized in signal analysis to look for patterns in data. Sample Entropy takes into consideration only force values which need to be sampled at equal intervals. Sample Entropy 2D, on the other hand, also accounts for the distances between points. Multiscale Sample Entropy extends the standard approach by analyzing the signal across multiple time scales. For computations, experimental results in the form of load-displacement diagrams for tensile tests performed on bone-shape samples are used. The experimental tests have been performed in room temperature for three strain rates. The band types are first identified based on DIC data by band movement observation. It is found that for a high strain rate we observe type A, for a medium strain rate first type A and then type B and for a low strain rate type C. The Sample Entropy and Sample Entropy 2d measures for type C are low and for type A are high. Different behavior of those two types is also visible for higher time scales. It is also found that to assess type B of PLC effect more experiments are needed.

Key words: Portevin Le-Chatelier effect, Multiscale Sample Entropy, Sample Entropy 2d

1. INTRODUCTION

In some materials, in a certain range of strain rates and temperatures, a propagative instability phenomenon called the Portevin Le Chatelier (PLC) effect occurs, [1,2,3]. Materials which exhibit such behavior are for example aluminum, [4], and steel, [5], where the PLC effect is visible in room temperature and elevated temperature, respectively. Other materials in which the phenomenon can be observed are Ni-based super alloys [6] and metal-matrix composited [7]. Characteristic for the PLC effect are serrations, repetitive changes from hardening to softening, visible in load-displacement diagram, and bands of plastic strain rate, associated with them, which occur in the sample. The PLC effect is linked to so-called Dynamic Strain Aging (DSA) and negative strain rate sensitivity. DSA is explained by plastic dislocation movement which is driven by plastic deformation. Dislocations can be stopped by defects in crystal grid, causing the material to strengthen (hardening) until the dislocations are freed and the stress drops (softening). The PLC bands are commonly observed during tensile tests, see e.g. [8], but also in shear [9,10]. More information about the micro-structural origin of this phenomenon can be found in [11] and in [12].

Three types of PLC effect are commonly distinguished: A, B and C, see for example [13,14]. They occur for different strain rates and temperatures, and are characterized by different behavior of propagating shear bands. Type A of PLC effect occurs in low temperature and for a high strain rate, the bands then propagate continuously. Type B can be observed for medium temperature and strain rate, the bands then have a tendency to hop. Type C occurs in high temperature and for a low strain rate, the bands then nucleate in a random manner. Sometimes different subtypes are distinguished, like types A1 and A2 in [15]. Authors of both [16] and [17] proved that an entropy measure called Sample Entropy (SampEn) can help recognize different PLC types, although their interpretations differ. In [16] SampEn for type A is high, for type B is medium and for type C has a low value. In [17] the entropy value is the largest for type B, lowest for type A and the value for type C is between the values for A and B. All values are relative because the SampEn measure depends on time step. A summary of these findings is presented in Tab. 1. The analysis of a similar entropy measure, namely the Refined Composite Multiscale Sample Entropy (RCMSE) for the PLC effect is provided in [18] and [19]. Although in [18] authors did not focus on PLC types and in [19] they only observed type C bands, they concluded that the Sample Entropy value is similar to the one from [16]. In the RCMSE the sample entropy for the original data is calculated in the same manner as the Sample Entropy in this article, but the methods differ for higher scales.

Tab. 1. PLC types considered in literature

PLC type	A	B	C
Temperature	low	medium	high
Strain rate	high	medium	low
Band movement	propagative	hopping	nucleating
Sarkar et al. 2010 [16]	high	medium	low
Xu et al. 2021 [17]	low	high	medium

The term entropy is used in many branches of science with many different definitions coming from the common concept of disorder measure. Here entropy is used for signal analysis, calculating how organized a signal is. The signal-type entropy was first introduced by Shannon in 1948 in [20], it is called Shannon Entropy. Many different entropy measures devoted to signals have been described since that time, see [21]. One of them is Sample Entropy (SampEn), see [22], and its extension Sample Entropy 2d (SampEn2d), see for example [23]. SampEn is a modification of Approximate Entropy [24] and can be used for shorter signals. These measures analyze patterns, looking for repetitiveness in data. A small value of entropy means that there are a lot of similar structures, as for a straight line or zig-zag, and a high value means that the data are chaotic. Entropy can be useful in different fields, for example in medicine [25,26], in image analysis [27] or even in stock market analysis [28].

A method proposed in [29] introduced a multiscale modification of entropy. It allows one to take into account different time scales for a complex time series. In the case of PLC effect it can provide additional information about serration and PLC type, see [16,17].

Entropy can also be a useful tool to improve material models by providing a way to compare experimental and numerical results in terms of load-displacement diagrams. It is not easy to say if two sets of serrations are similar, but having one value characterizing them can be helpful in this respect. Many models have been proposed to simulate the PLC-type behavior, for example the Estrin-McCormick model [30,31,32], the model created by Wang [33] or the model based on thermodynamic features [34].

The goal of this article is to verify the results from [16] and [17]. Moreover, the article includes a comprehensive analysis of the sample entropy calculation for the PLC effect, along with a detailed discussion of its drawbacks, and a description of the algorithms used with new experimental data for different strain rates. Moreover, a different method is proposed, which is not sensitive to time step.

The present article is structured as follows. Section 2 outlines the used methods with examples, namely the Sample Entropy, Sample Entropy 2d and Multiscale Sample Entropy. Section 3 contains the results of experiments of the Portevin-Le Chatelier effect. Chapter 4 provides a summary and conclusions.

2. ENTROPY

In this section the algorithms of calculating entropy measures are introduced. First the Sample Entropy [22], then Sample Entropy 2d [23], and finally Multiscale Sample Entropy [29] are outlined. All methods are focused on patterns, the first one uses one-dimensional data in equal intervals and the second one employs two-dimensional data, the third is an extension of Sample Entropy. For SampEn and SampEn2d the description boxes with algorithms are provided in Appendix 1, and for all measures some example calculations are performed.

Example calculations are performed for data generated numerically for a white, pink or brown noise, which are frequently used to present the Sample Entropy method. If not stated otherwise, 1000 data points are generated.

2.1. Sample Entropy

Sample Entropy [22] is an algorithm focused on finding patterns in a time series. First, time series X in equal intervals is divided into *m*-elements and *m+1*-elements vectors, $Y_i^m = (x_i, x_{i+1}, \dots, x_{i+m-1})$. Parameter m is called an embedded dimension and is usually equal to 2. The next step is to calculate a maximum norm of the distance between vectors and compare it with tolerance r. The tolerance is a percentage of standard deviation, usually around 20 % (in the case of this article the tolerance is set to 15 %). The events when the maximum norm is smaller than the tolerance have to be counted and stored in variable n_m. Next, the steps are repeated for $m+1$ and variable n_{m+1} is the result. The sample entropy is equal to natural logarithm of the fraction of n_m divided by n_{m+1}. Calculating the Sample Entropy is summarized in Alg. 1 in Appendix 1.

To assess the Sample Entropy measure some calculations for a white noise are provided. The first task is to check how many points are required to obtain reliable results. Files with different numbers of points are generated and the calculation of Sample Entropy is performed. For each case 100 files are generated (with the exception of 10000 points where only 10 files are generated) and four values are provided, maximum, minimum, mean and standard deviation. The results are summarized in Tab. 2. Based on the calculations of standard deviation, it can be seen that the results for 800 points are reliable for Sample Entropy calculation which is consistent with the value reported in [22].

Tab. 2. Sample Entropy for White Noise

No. of points	Mean	Std. dev	Min	Max
100	2.58	0.59	1.49	3.81
300	2.51	0.19	2.13	2.94
500	2.47	0.12	2.22	2.79
600	2.49	0.10	2.25	2.70
700	2.47	0.09	2.29	2.72
800	2.49	0.066	2.34	2.65
900	2.48	0.059	2.35	2.61
1000	2.48	0.055	2.35	2.62
2000	2.47	0.033	2.37	2.57
10000	2.47	0.0069	2.46	2.49

Sample Entropy, however, has some limitations which have to be addressed. First of all the data need to be in equal intervals, which impedes using data from computations with an adaptive time step. Another issue is sensitivity to the step size, since only the values calculated for the same steps can be compared with each other. To illustrate this, let us calculate SampEn for a white noise. The white noise can be generated using normal Gauss distribution, in this case 1000 points are generated. The sample entropy value for the white noise oscillates around 2.5 and for this particular calculation it is equal to 2.59. Let us interpolate between existing values, now SampEn is equal to 0.58. Another problem is data with a trend. Now, function x^2 is added to the previously used white noise.

DOI 10.2478/ama-2025-0080

Let us assume that the distance between data points is one. The Sample Entropy for the data with the trend is equal to 0.00347. In the case of different time steps the solution is interpolation and the trend can be removed by fitting a suitable function. This however means that apart from additional work some information can be lost in the process. Sample Entropy calculations are also time consuming. All of method characteristics make it impossible to formulate objective ranges for different PLC types.

2.2. Sample Entropy 2d for normalized data

To avoid some problems characteristic for the Sample Entropy another method is used. The algorithm called Sample Entropy 2d [23] is very similar to the Sample Entropy, but calculations are performed for a two-dimensional time series (X, Y), see Appendix 1 Alg. 2. The tolerance r is now set as

$$r = p\sqrt{S_x^2 + S_y^2} \tag{1}$$

where p is usually equal to 0.3, [23] and the geometric mean of the standard deviations for the x and y values is used.

To avoid problems with one dimension dominating, which happens for the values of X, some additional steps are proposed. Only the values for local extremes are selected and the values of Y are moved to the beginning of the coordinate system (Y becomes a set of distances between extremes). Next the data are normalized using the equations:

$$x = \frac{x_i - x_{min}}{x_{max} - x_{min}}, \qquad y = \frac{y_i - y_{min}}{y_{max} - y_{min}} \tag{2}$$

The normalized data are used for calculating Sample Entropy 2d. All steps are presented in Appendix 1, Alg. 2.

Similarly to Sample Entropy, the calculations of Sample Entropy 2d are performed for a white noise and summarized in Tab. 3. One hundred sets of data are generated for each case (with the exception of 10000 points where 10 files are generated).

Tab. 3. Sample Entropy 2d for white noise

No. of points	Mean	Std. dev	Min	Max
100	0.84	0.22	0.47	1.88
300	0.76	0.10	0.54	1.05
500	0.77	0.093	0.54	1.02
700	0.76	0.078	0.58	0.94
800	0.74	0.072	0.61	0.95
900	0.75	0.06	0.59	0.88
1000	0.76	0.06	0.59	0.9
2000	0.75	0.047	0.65	0.87
10000	0.75	0.028	0.72	0.8

2.3. Multiscale Sample Entropy

Multiscale Sample Entropy (MSE) [29] provides additional insight into different time scales for a complex time series. This modification introduces time scale factor τ. The original time series $X = \{x_1, x_2, \ldots, x_N\}$ with N values needs recalculation using a so-called coarse-grain method, see Fig. 1.

$$Y^\tau = \frac{1}{\tau}\sum_{i=j}^{j+\tau-1} x_i\,, 1 \le j \le N - \tau + 1 \tag{3}$$

Multiscale Sample Entropy for different scale factors is calculated exactly like Sample Entropy in 2.1, but for the time series obtained from Eq. 3. When τ is equal to 1, the time series is equal to the original times series X. The coarse-grain method works as follows. Time series $X = \{1,2,3,4,5,6,7,8,9,10\}$ is given. For $\tau = 2$, the new time series is equal to $Y^2 = \{\frac{1+2}{2}, \frac{3+4}{2}, \frac{5+6}{2}, \frac{7+8}{2}, \frac{9+10}{2}\} = \{1.5,3.5,5.5,7.5,9.5\}$.

Calculations for a white noise, brown noise and pink noise are provided in Fig. 2. It can be observed that each noise has its characteristic MSE behavior. SampEn for the white noise drops when the scale parameter grows – complexity for higher time scales drops, SampEn for the pink noise is approximately constant – the same complexity for all time scales considered and SampEn for the brown noise rises – complexity also increases.

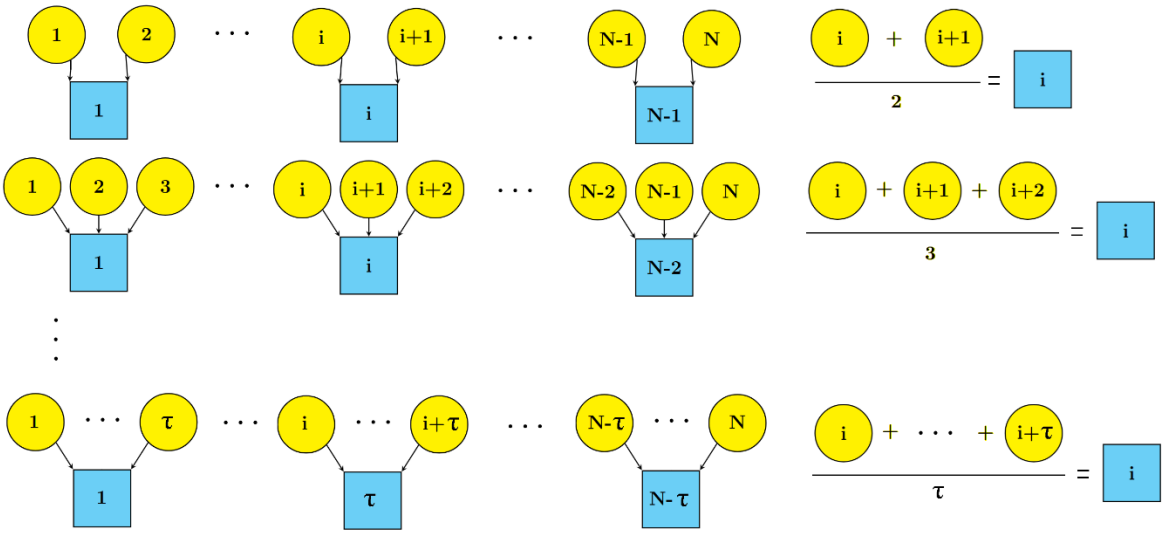

Fig. 1. Visualization of coarse-grain method

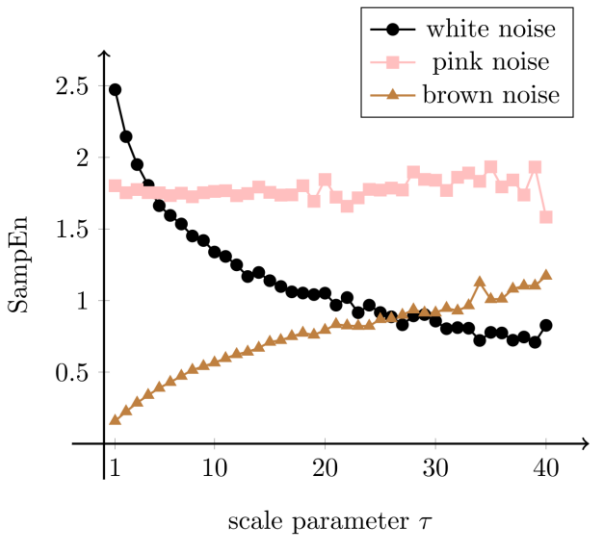

Fig. 2. Sample Entropy for different scale parameters

3. RESULTS FOR PLC EFFECT

In this section calculations for the Portevin-Le Chatelier effect using data published previously in [35] are shown. First, the experimental results are introduced with additional observations made for DIC images. Next, the computations of Sample Entropy, Sample Entropy 2d and Multiscale Sample Entropy are outlined similarly to the previous section. Contrary to the white noise data, the experimental data have a trend, hence the first step is to fit function $f(x) = a + b\,e^{-x}$ to the time series and subtract the fitted values from the experimental ones. The prepared data are then used for SampEn, SampEn2d and MSE computations.

3.1. Experimental data

In Fig. 3 plots of the sum of reactions vs. time are shown for different strain rates and room temperature. For visibility reason the lines are shifted by 3 MPa. Experiments are performed for bone shape samples with active zone dimensions: 102 mm length, 25 mm width and 2 mm thickness. Nine samples are used, three for each strain rate. Samples number 1, 2 and 3 are stretched with strain rate equal to 4.3×10^{-4} (low strain rate), samples 4, 5 and 6 with strain rate equal to 4.3×10^{-3} (medium strain rate) and samples 7, 8, 9 with strain rate equal to 4.3×10^{-2} (high strain rate).

Strain rate bands appearing during loading are characteristic for particular PLC types. For different PLC types different band movement is observed. The A type bands travel/propagate, type B bands jump/hop and C type bands nucleate randomly. Based on DIC observations PLC types are assigned to every set of experiments, see Tab. 4. For the low strain rate (experiments 1,2,3) the bands were nucleating which indicated type C, for the medium strain rate the bands were first traveling/propagating continuously which indicated the first type A and then they were hopping which indicated type B. For the high strain rate the bands were propagating, which again indicated type A. In Fig. 3 for the medium strain rate the point where the type changed from A to B is visible around time 18 s, see Fig. 3 d. The process has a transient character when serration change shape and size.

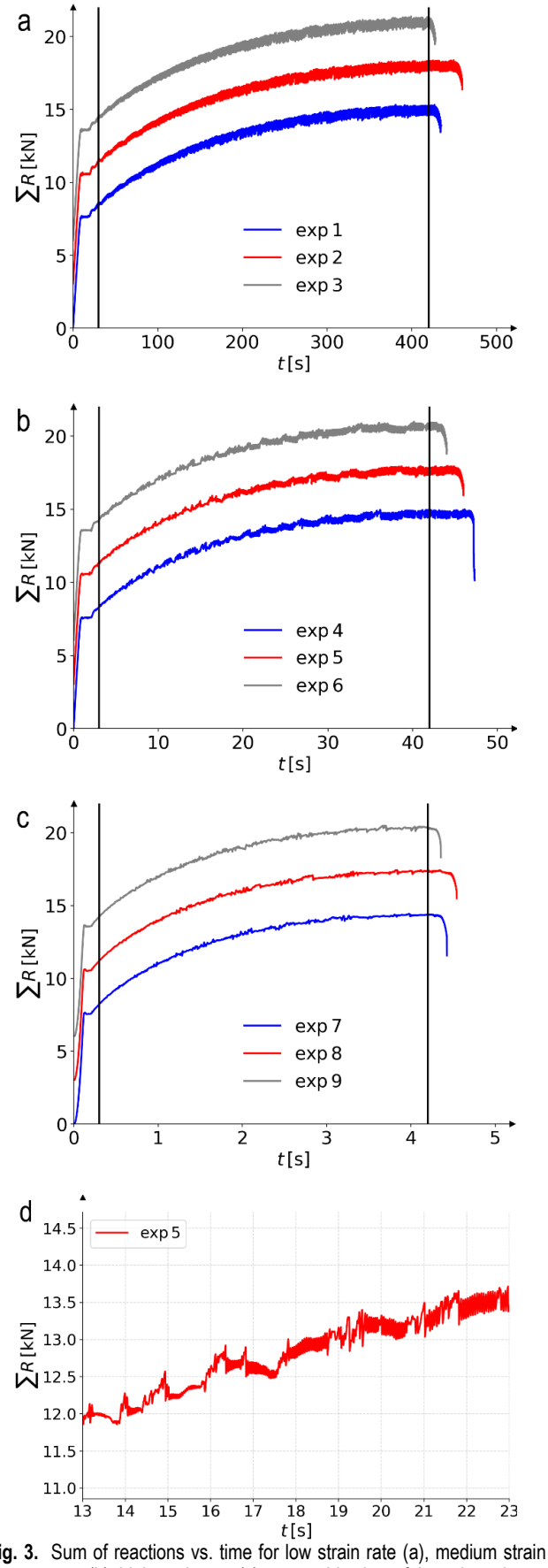

Fig. 3. Sum of reactions vs. time for low strain rate (a), medium strain rate (b), high strain rate (c), zoomed-in view of the selected area for medium strain rate (d)

DOI 10.2478/ama-2025-0080

Tab. 4. Observation summary of DIC data

Strain rate	Bands behavior	PLC type
Low	nucleating	C
Medium	travelling and hopping	A+B
High	travelling	A

3.2. Results for Sample Entropy

The results for Sample Entropy are summarized in two tables. In Tab. 5 the results for SampEn measure for the range marked by black lines in Fig. 3 are displayed. The samples number 1 to 3 are for the low strain rate, the samples number 4 to 6 are for the medium strain rate, and 7 to 9 for the high strain rate. In Tab. 6 the results for the medium strain rate for two sets of data ranging from 3 s to 13 s (SampEnA) and from 32 s to 42 s (SampEnB) are shown. The distinction is made to check if the values of Sample Entropy differ and are consistent with DIC observation (first type A and then B). The results are summarized in Fig. 4.

The PLC classification is known from the DIC data (see Tab. 4). For the low strain rate (samples 1,2,3) we observe type C, for which entropy is the lowest. The low entropy value indicates that serrations are more organized than for the other samples. In the case of high strain rate (samples 7,8,9) SampEn has the highest value, serrations are more chaotic than for the other samples. For the medium strain rate (samples 5,6,7) the movement of bands changes during the process. First type A bands are visible, then type B. The values of SampEnB are similar to the values of SampEn calculated for the range 3 s to 42 s, but the values of SampEnA are closer to the values for samples 1,2,3 (where type C can be spotted) than to the values for type A. The experiments where only B type is visible are needed to verify results. The results are summarized in Fig. 4.

These results are consistent with [16], where type A bands have the highest SampEn, type C the lowest, and type B values are in between. In [17], type A bands have the lowest SampEn, type B the highest, and type C values are intermediate.

Tab. 5. Sample Entropy for PLC effect and equal time steps (0.001s)

Sumple no.	SampEn
1	0.01967
2	0.01475
3	0.01448
4	0.12021
5	0.12062
6	0.12557
7	0.23605
8	0.25310
9	0.29345

Tab. 6. Sample Entropy for medium strain rate, equal time steps (0.001s), range 3 s to 13 s (SampEnA) and range of 32 s to 42 s (SampEnB)

Sumple no.	SampEnA	SampEnB
4	0.05232	0.12640
5	0.04391	0.11078
6	0.06010	0.13207

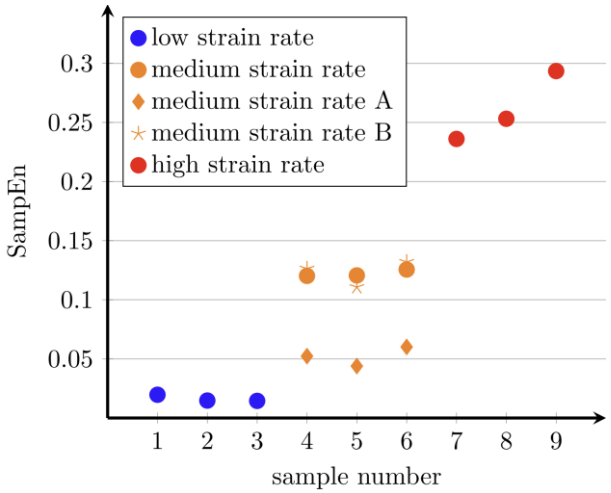

Fig. 4. Sample Entropy for PLC effect and equal time steps (0.001s). Summary for Tabs. 5 and 6

3.3. Results for Sample Entropy 2d and normalized data

The values of Sample Entropy 2d are summarized in Tab. 7 and Fig. 5. The results for low and medium strain rates are on the same level, between 0.5 and 1.5, and for the high strain rate around 3.0-3.5. It indicates a similar tendency as for Sample Entropy. There is not enough data to calculate SampEn2d for two intervals as for SampEn.

Tab. 7. Sample Entropy 2d for PLC effect

Sumple no.	SampEn
1	1.09861
2	0.68253
3	0.72350
4	0.91049
5	0.97507
6	1.29142
7	3.84859
8	3.00294
9	x

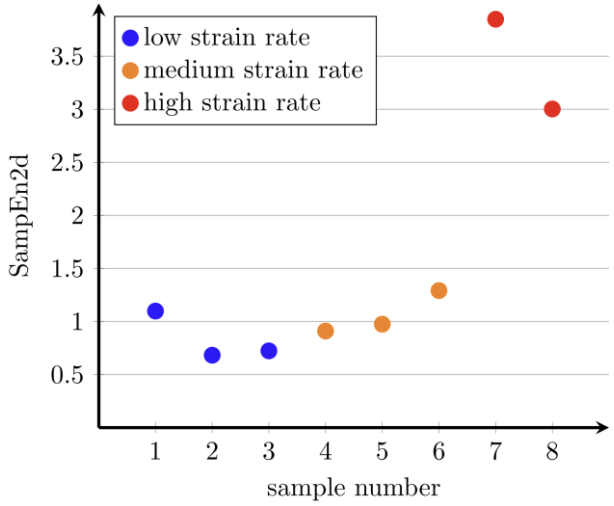

Fig. 5. Sample Entropy 2d for PLC effect

3.4. Results for Multiscale Sample Entropy

Multiscale Sample Entropy reflects the complexity of a signal at higher time scales. In Fig. 6 the results for MSE and different strain rates are drawn. In the case of low strain rate SampEn rises linearly in a steady manner when the scale parameter grows. The complexity of the signal is higher for higher time scales. For the medium strain rate SampEn first rises linearly and the diagram is steeper than the low strain rate line. When parameter τ is close to 20 the diagram starts to drop slightly and then slowly rises again when the scaling parameter is close to 60. The signal complexity changes, for smaller scales it is more complex and then it is almost stable. For the high strain rate SampEn rises with almost the same tangent as for the medium strain rate but the diagram is strongly non-linear. After τ reaches 20 the SampEn values start to jump, it can be caused by too little data since when τ grows the number of data decreases. This is also the reason why not all values are available for a high scaling parameter. Additional computations are carried out for partial data for the medium strain rate, namely from 3 s to 13 s (called A) and from 32 s to 42 s (called B). This shows different serration types, see Tab. 4. In case A the Sample Entropy values rise similarly to case B and full data. Around τ equal to 10 the inclination of the diagram starts to decrease and around 30 the values of SampEn start to jump. In case B the SampEn values rise with a similar tangent as for full data, then around τ equal to 25 the diagram starts to drop and around 40 the values start to jump. All strain rates show similar trends, the complexity of the time series rises at the beginning.

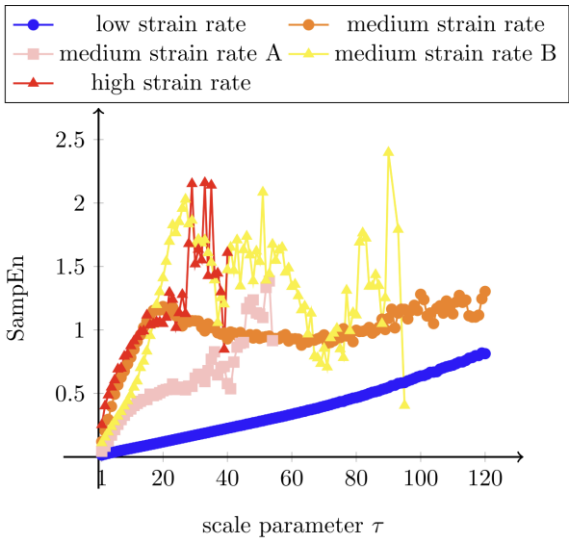

Fig. 6. Sample Entropy for different scale parameters

In the case of [16] MSE for C type bands behaves in a similar way to low strain rate (also identified as C type bands) when the complexity slightly rises (note that the authors of [16] calculated MSE for a scale factor below 21). In [16] for B type bands MSE first rises then drops and for A type bands MSE first drops then rises with some fluctuations. The B type behavior is similar to medium strain rate from this article without fluctuations. Different behavior for A type bands (in this article line is rising) can be caused by different frequency with which the signal is saved.

In [17] MSE for A type bands behaves in a similar way as for the low strain rate (here C type bands) – the complexity of time series steadily rises, although much slower than for other PLC types. In [17] for B and C type bands MSE first rises then drops and saturates. In this article a similar behavior is observed for medium strain rate with a mix of A and B type bands and "medium strain rate B" without fluctuations. However, in [17] the drop is more significant comparing to the medium strain rate from this article.

Based on the MSE analysis we can clearly distinguish between type C (as suggested by DIC images) for the low strain rate and types A and B for the high and medium strain rates. It is more difficult to separate types A and B. The band C serrations are less chaotic then B and A for all scales. More tests with bands of those types are needed.

4. CONCLUSIONS

This article deals with the calculation of entropy measures to distinguish between different PLC band types on the basis of load-displacement data. The data have been taken from experiments on bone-shape samples in tension, which were made for three strain rates (low, medium and high). Three sets of entropy computations have been performed using three measures: Sample Entropy, Sample Entropy 2d and Multiscale Sample Entropy. Based on DIC results and strain rate band movement it can be stated that for the low strain rate shear bands of type C are observed, for the medium strain rate first of type A and then type B, and for the high strain rate bands of type A are noticed. It has been found that Sample Entropy and Sample Entropy 2d are low for the low strain rate, indicating that serrations are more organized than for the other strain rates. For the high strain rate the entropy measures are high, which shows that the serrations are more chaotic than for the medium and low strain rates. The Sample Entropy for the medium strain rate is between the values for the low and high strain rate, but the DIC data show that two band types are visible, so additional computations are carried out for the data at the beginning and at the end of the loading process. The values from the beginning are close to the values for type C bands, however DIC shows type A bands. The values from the end of the process are similar to the values for the whole process. The value of Sample Entropy 2d for the medium strain rate is close to the values for the low strain rate. The results for bands of type A and C are consistent with those presented in [16]. The values of Multiscale Sample Entropy show a clear difference between the low strain rate (type C) on one hand and the medium and high strain rates (types A and B) on the other hand. The MSE for type C bands and, to a lesser extent, for type B bands also presents a similar behavior to the one from [16]. It is hard to find a clear difference between types A and B on the basis of those computations. It is also possible that the classification based on DIC data is not precise enough except for type C bands, hence more experiments showing clearly types A and B are needed. The results are summarized in Tab. 8.

Tab. 8. Results summary for PLC types

PLC type	A	B	C
Temperature	low	medium	high
Strain rate	high	medium	low
Band movement	propagative	hopping	nucleating
Sarkar et al. 2010 [16]	high	medium	low
Xu et al. 2021 [17]	low	high	medium
SampEn	high	medium	low
SampEn2d	high	-	low

DOI 10.2478/ama-2025-0080

Appendix 1

This appendix contains Algorithms for Sample Entropy (Alg. 1) and Sample Entropy 2d (Alg. 2).

Alg. 1. Sample Entropy Algorithm

Require: time series data $X = \{x_1, x_2, \ldots, x_N\}$, embedded dimension $m = 2$, tolerance $r = 0.15\ S_X$

Initialize $n_2 \leftarrow 0, n_3 \leftarrow 0$
for $i = 1$ to $N - m + 1$ **do**
    Compute m-dimensional vectors: $Y2(:, i) = (x_i, x_{i+1})$
end for
for $i = 1$ to $N - m - 1$ **do**
    for $j = i + 1$ to $N - m$ **do**
        Compute max norm $d = \max |Y2_{:,i} - Y2_{:,j}|$
        if $d < r$ **then**
            $n_2 \leftarrow n_2 + 1$
        end if
    end for
end for
$m \leftarrow m + 1$
for $i = 1$ to $N - m + 1$ **do**
    Compute m-dimensional vectors: $Y3(:, i) = (x_i, x_{i+1}, x_{i+2})$
end for
for $i = 1$ to $N - m - 1$ **do**
    for $j = i + 1$ to $N - m$ **do**
        Compute max norm $d = \max |Y3_{:,i} - Y3_{:,j}|$
        if $d < r$ **then**
            $n_3 \leftarrow n_3 + 1$
        end if
    end for
end for
Compute $SampEn \leftarrow \ln \frac{n_2}{n_3}$

Alg. 2. Sample Entropy 2d Algorithm for normalized data

Require: time series data $(X, Y) = \{\{x_1, y_1\}, \{x_2, y_2\}, \ldots, \{x_N, y_N\}\}$, embedded dimension $m = 2$, tolerance $r = 0.3\sqrt{S_X^2 + S_Y^2}$

Move Y **value to the beginning of coordinate system**
for $i = 2$ to N **do**
    $y' = y_i - y_{i-1}$
end for
Normalize data
for $i = 1$ to N **do**
    $x_{n,i} = \frac{x_i - x_{min}}{x_{max} - x_{min}}$
    $y_{n,i} = \frac{y'_i - y'_{min}}{y'_{max} - y'_{min}}$
end for
Initialize $n_2 \leftarrow 0, n_3 \leftarrow 0$

for $i = 1$ to $N - m + 1$ **do**
    Compute m-dimensional vectors: $Y2(:, i) = (\{x_{n,i}, y_{n,i}\}, \{x_{n,i+1}, y_{n,i+1}\})$
end for
for $i = 1$ to $N - m - 1$ **do**
    for $j = i + 1$ to $N - m$ **do**
        Compute max norm $d = \max |Y2_{:,i} - Y2_{:,j}|$
        if $d < r$ **then**
            $n_2 \leftarrow n_2 + 1$
        end if
    end for
end for
$m \leftarrow m + 1$
for $i = 1$ to $N - m + 1$ **do**
    Compute m-dimensional vectors: $Y3(:, i) = (\{x_{n,i}, y_{ni}\}, \{x_{n,i+1}, y_{n,i+1}\}, \{x_{n,i+2}, y_{n,i+2}\})$
end for
for $i = 1$ to $N - m - 1$ **do**
    for $j = i + 1$ to $N - m$ **do**
        Compute max norm $d = \max |Y3_{:,i} - Y3_{:,j}|$
        if $d < r$ **then**
            $n_3 \leftarrow n_3 + 1$
        end if
    end for
end for
Compute $SampEn \leftarrow \ln \frac{n_2}{n_3}$

REFERENCES

1. Portevin A, Le Chatelier F. Sur un phénomène observé lors de l'essai de traction d'alliages en cours de transformation. Compt Rend Acad Sci Paris. 1923;176:507-510.
2. Bergstrom Y, Roberts W. The application of dislocation model to dynamic strain ageing in α-iron containing interstitial atoms. Acta Metall. 1971;19:815-823. https://doi.org/10.1016/0001-6160(71)90138-6
3. Yilmaz A. The Portevin-Le Chatelier effect: a review of experimental findings. Sci Technol Adv Mater. 2011;12(6). https://doi.org/10.1088/1468-6996/12/6/063001
4. Reyne B, Manach PY, Moës N. Macroscopic consequences of Piobert–Lüders and Portevin–Le Chatelier bands during tensile deformation in Al-Mg alloys. Mater Sci Eng A. 2019;746:187-196. https://doi.org/10.1016/j.msea.2019.01.009
5. Sarkar A, Maloy SA, Murty KL. Investigation of Portevin-Le Chatelier effect in HT-9 steel. Mater Sci Eng A. 2015;631:120-125. https://doi.org/10.1016/j.msea.2015.02.022
6. Cui C, Zhang R, Zhou Y, Sun X. Portevin-Le Châtelier effect in wrought Ni-based superalloys: Experiments and mechanisms. J Mater Sci Technol. 2020;51:16-31. https://doi.org/10.1016/j.jmst.2020.03.023
7. Graff S, Dierke H, Forest S, Neuhäuser H, Strudel JL. Finite element simulations of the Portevin–Le Chatelier effect in metal–matrix composites. Philos Mag. 2008;88:3389–3414. https://doi.org/10.1080/14786430802108472
8. Lipski A, Mroziński S. The effects of temperature on the strength properties of aluminium alloy 2024-T3. Acta Mech Autom. 2012;6(3):62-66.
9. Coër J, Manach PY, Laurent H, Oliveira MC, Menezes LF. Piobert–Lüders plateau and Portevin–Le Chatelier effect in an Al–Mg alloy in simple shear. Mech Res Commun. 2013;48:1-7. https://doi.org/10.1016/j.mechrescom.2012.11.008
10. Manach PY, Thuillier S, Yoon JW, Coër J, Laurent H. Kinematics of Portevin-Le Chatelier bands in simple shear. Int J Plast. 2014;58:66-83. https://doi.org/10.1016/j.ijplas.2014.02.005
11. Cottrell AH, Bilby BA. Dislocation theory of yielding and strain ageing of iron. Proc Phys Soc A. 1949;62(1):49-62. https://doi.org/10.1088/0370-1298/62/1/308
12. Kozłowska A, Grzegorczyk B, Morawiec M, Grajcar A. Explanation of the PLC Effect in Advanced High-Strength Medium-Mn Steels. A Review. Materials. 2019;12(24):1-14. https://doi.org/10.3390/ma12244175
13. Jiang H, Zhang Q, Chen X, Chen Z, Jiang Z, Wu X, Fan J. Three types of Portevin–Le Chatelier effects: Experiment and modelling. Acta Mater. 2007;55(7):2219-2228. https://doi.org/10.1016/j.actamat.2006.10.029
14. Hu Q, Zhang Q, Cao P, Fu S. Thermal analyses and simulations of the type A and type B Portevin–Le Chatelier effects in an Al–Mg alloy. Acta Mater. 2012;60(4):1647-1657. https://doi.org/10.1016/j.actamat.2011.12.003
15. Schwink CH, Nortmann A. The present experimental knowledge of dynamic strain ageing in binary f.c.c. solid solutions. Mater Sci Eng A. 1997;234:1-7. https://doi.org/10.1016/S0921-5093(97)00139-1

DOI 10.2478/ama-2025-0080

16. Sarkar A, Barat P, Mukherjee P. Multiscale entropy analysis of the Portevin-Le Chatelier Effect in an Al-2.5%Mg alloy. Fractals. 2010;18:319-325. https://doi.org/10.1142/S0218348X10004944
17. Xu J, Chen G, Fu S. Complexity analysis of the Portevin-Le Chatelier in an Al alloy at different temperatures. Theor Appl Mech Lett. 2021;11(2):100233. https://doi.org/10.1016/j.taml.2021.100233
18. Brechtl J, Xie X, Wang Z, Qiao J, Liaw PK. Complexity analysis of serrated flows in a bulk metallic glass under constrained and unconstrained conditions. Mater Sci Eng A. 2020;771:138585. https://doi.org/10.1016/j.msea.2019.138585
19. Brechtl J, Chen B, Xie X, Ren Y, Venable JD, Liaw PK, Zinkle SJ. Entropy modeling on serrated flows in carburized steels. Mater Sci Eng A. 2019;753:135-145. https://doi.org/10.1016/j.msea.2019.02.096
20. Shannon CE. A mathematical theory of communication. Bell Syst Tech J. 1948;27(3):379-423. https://doi.org/10.1002/j.1538-7305.1948.tb01338.x
21. Namdari A, Li Z. A review of entropy measures for uncertainty quantification of stochastic processes. Adv Mech Eng. 2019;11:1-14. https://doi.org/10.1177/1687814019857
22. Richman JS, Moorman JR. Physiological time-series analysis using approximate entropy and sample entropy. Am J Physiol Heart Circ Physiol. 2000;278: H2039–H2049. https://doi.org/10.1152/ajpheart.2000.278.6.H203
23. Wu H, Zhou J, Xie C, Zhang J, Huang Y. Two-Dimensional Time Series Sample Entropy Algorithm: Applications to Rotor Axis Orbit Feature Identification. Mech Syst Signal Process. 2021;147:107123. https://doi.org/10.1016/j.ymssp.2020.107123
24. Pincus SM. Approximate entropy as a measure of system complexity. Proc Natl Acad Sci U S A. 1991;88:2297–2301. https://doi.org/10.1073/pnas.88.6.229
25. Mayer CC, Bachler M, Hörtenhuber M, Stocker C, Holzinger A, Wassertheurer S. Selection of entropy-measure parameters for knowledge discovery in heart rate variability data. BMC Bioinformatics. 2014;15(6):S2. https://doi.org/10.1186/1471-2105-15-S6-S2
26. Trybek P, Nowakowski M, Salowka J, Spiechowicz J, Machura L. Sample Entropy of sEMG Signals at Different Stages of Rectal Cancer Treatment. Entropy. 2018;20:863. https://doi.org/10.3390/e20110863
27. Azami H, da Silva LEV, Omoto ACM, Humeau-Heurtier A. Two-dimensional dispersion entropy: An information-theoretic method for irregularity analysis of images. Signal Process Image Commun. 2019;75:178-187. https://doi.org/10.1016/j.image.2019.04.013
28. Olbryś J, Majewska E. Regularity in Stock Market Indices within Turbulence Periods: The Sample Entropy Approach. Entropy. 2022;24:921. https://doi.org/10.3390/e24070921
29. Costa M, Goldberger AL, Peng CK. Multiscale Entropy Analysis of Complex Physiologic Time Series. Phys Rev Lett. 2002;89:068102. https://doi.org/10.1103/PhysRevLett.89.068102
30. McCormick PG. Theory of flow localization due to dynamic strain aging. Acta Metall. 1988;36(12):3061-3067. https://doi.org/10.1016/0001-6160(88)90043-0
31. Zhang S, McCormick PG, Estrin Y. The morphology of Portevin-Le Chatelier bands: Finite element simulation for Al-Mg-Si. Acta Mater. 2001;49(6):1087-1094. https://doi.org/10.1016/S1359-6454(00)00380-3
32. Böhlke T, Bondár G, Estrin Y, Lebyodkin MA. Geometrically nonlinear modeling of the Portevin-Le Chatelier effect. Comput Mater Sci. 2009;44(4):1076-1088. https://doi.org/10.1016/j.commatsci.2008.07.036
33. Wang WM. Stationary and propagative instabilities in metals: a computational point of view [dissertation]. Delft: Delft University of Technology; 1997.
34. Hähner P, Rizzi E. On the kinematics of Portevin–Le Chatelier bands: theoretical and numerical modelling. Acta Mater. 2003;51(12):3385-3397. https://doi.org/10.1016/S1359-6454(03)00122-8
35. Mucha M, Rose L, Wcisło B, Menzel A, Pamin J. Experiments and numerical simulations of Lueders bands and Portevin-Le Chatelier effect in aluminium alloy AW5083. Arch Mech. 2023;75(3):301-336. https://doi.org/10.24423/aom.4204

The work is supported within Weave-UNISONO call by the German Research Foundation (DFG grant 527828607) and by the National Science Center, Poland (NCN grant 2023/05/Y/ST8/00006). The author are grateful to prof. Jerzy Pamin, prof. Andreas Menzel and dr Lars Rose for their helpful comments on this article.

Marzena Mucha https://orcid.org/0000-0001-9667-6045